applied sciences

MDPI

Article

Performance Evaluation of an Imaging Radiation Portal Monitor System

Jana Vasiljević * and Bo Cederwall *

Department of Physics, KTH Royal Institute of Technology, SE 10691 Stockholm, Sweden
* Correspondence: janape@kth.se (J.V.); bc@kth.se (B.C.)

Abstract: An organic scintillator-based radiation portal monitor (RPM) prototype system with imaging capabilities has been developed based on the neutron–gamma emission tomography technique. The technique enables rapid detection and precise location of small amounts of special nuclear materials, such as plutonium, using time and energy correlations between fast neutrons and gamma rays from spontaneous fission with low false-alarm rates. These capabilities, in addition to state-of-the-art detection of various gamma-emitting sources, enables the novel imaging RPM concept to efficiently address global security threats from terrorism and the proliferation of nuclear weapons. The detector approach is simple and versatile and can easily be adapted for different applications in nuclear security, public safety, nuclear emergency response, and radiological surveying. In this work, basic performance parameters of the imaging RPM prototype system developed at KTH have been evaluated.

Keywords: radiation portal monitor; organic scintillator; radiation imaging; neutron and gamma detection; special nuclear materials

check for updates

Citation: Vasiljević, J.; Cederwall, B. Performance Evaluation of an Imaging Radiation Portal Monitor System. *Appl. Sci.* **2022**, *12*, 9001. https://doi.org/10.3390/app12189001

Academic Editor: Jeong Ik Lee

Received: 19 August 2022
Accepted: 6 September 2022
Published: 7 September 2022

1. Introduction

The trafficking of special nuclear materials (SNM), such as weapons-grade plutonium (WGP) and highly enriched uranium (HEU), or other radioactive materials that could be used as radiological dispersion devices or contribute to the proliferation of nuclear weapons, remains one of the main global security challenges. The IAEA Incident Trafficking Database (ITDB) 2020 Fact Sheet reported 290 incidents between 1993 and 2019 that involved confirmed or probable acts of trafficking or malicious use [1]. It is quite possible that the number of detected incidents represents a relatively small fraction of such events. Therefore, improvements in the sensitive detection and rapid location of illicit radiation sources during screening of individuals, vehicles, or cargo at security check points at borders or at secure facilities is of fundamental importance for public safety.

We have previously reported on a new technique, neutron-gamma emission tomography (NGET) [2,3], for efficient 3D location of SNM within the field of view of a radiation portal monitor (RPM) system based on organic scintillators. The NGET technique is versatile and can easily be adapted to different detection geometries in different applications in nuclear security, public safety, nuclear emergency response, radiological surveying, etc. It uses correlations in time, space, and energy between fast neutrons and gamma rays from spontaneous or induced fission, providing a novel radiation imaging modality as well as enhanced detection sensitivity for SNM with low false alarm rates. While our previous efforts were focused on demonstrating the proof-of-principle of the NGET technique, in this study, we evaluate the detection and localization capabilities of an imaging RPM in more realistic conditions, in particular with respect to shielding materials.

Our results are presented in the following order. In Section 2 the detection system (Section 2.1) and the application of the NGET method (Section 2.2) are described. The RPM performance is reported in Section 3. Section 4 presents the results of NGET localization of

SNM. The results and future research directions indicated by this work are discussed in Section 5.

2. Materials and Methods

2.1. Detection System

Radiation portal monitors are installed at nuclear facilities, air and seaports, border crossings, cargo terminals, etc. to screen persons, vehicles, and other objects in order to detect and prevent the trafficking of radioactive materials. Basic systems are sensitive only to gamma-emitting radioactive sources, while the detection of plutonium and other types of SNM also warrants detection of neutrons. Currently, the most commonly used neutron detectors in nuclear safeguards and security systems, such as RPMs, are ^{3}He thermal neutron gaseous proportional counters [4,5]. Nevertheless, there is a rising interest in replacing ^{3}He detectors with other technologies driven by the global shortage of ^{3}He [6]. Besides replacing ^{3}He with other high-neutron-absorption cross-section materials for thermal neutrons like boron and lithium, there is also an increasing focus on fast-neutron detection using organic scintillators, high-pressure ^{4}He systems [7], etc. Organic scintillators have been found to be competitive alternatives in terms of intrinsic detection efficiency compared with with the "gold standard" ^{3}He-based systems [8]. Furthermore, while thermal or epithermal neutrons typically have scattered multiple times in surrounding materials on their way from the source, fast neutrons preserve some direct information about the initial emission process and its location. Thanks to their generally excellent timing properties this leads to key advantages for organic scintillator-based detection systems for background suppression and selectivity by using fast time correlations between the detected particles.

The phase I RPM prototype system developed at KTH consists of eight organic scintillator detector cells, placed in two vertical pillars (see Figure 1). The current mechanical support structure is adapted to the ANSI N42.35-2016 industry standard [9] and is suitable for different package (or conveyor) and pedestrian RPMs, but it can easily be modified to different scenarios and applications. The mechanical structure can support up to 50 detector cells, 20 horizontally oriented in each pillar and 10 detector cells at the top of the structure. Organic scintillators were chosen as detection medium because they are sensitive to both gamma rays and fast neutrons with high efficiency and are available with pulse-shape discrimination (PSD) capabilities for distinguishing between the two types of particles. In addition, organic scintillators typically have excellent timing properties, of the order of 1 ns or better (FWHM), depending on the particle energies, detector geometry, and the properties of the sensors used for reading out the scintillation light.

In the current configuration of the KTH Phase I RPM prototype system, detector cells of cylindrical shape with 127 mm diameter by 127 mm length were mounted in a zig-zag pattern in the mechanical support structure. This configuration is rather compact and was adapted for use in radioactive waste scanning applications. It therefore conforms most closely to the package/conveyor RPM category specified in the ANSI N42.35-2016 standard document. Each detector cell contains approximately 1.6 l of EJ-309 liquid organic scintillator [10] and it is optically coupled to a Hamamatsu R1250 photomultiplier tube (PMT). The PMTs are powered by two four-channel CAEN DT5533 high-voltage power supplies and their anode pulses were collected and digitized using an eight-channel CAEN DT5730 digitizer board. The digitizer board has a 2-Vpp dynamic range, 14-bit resolution, 500 MHz sampling rate, and features firmware programmable PSD capabilities for distinguishing between gamma rays and neutrons using field programmable gate arrays (FPGA). The PSD algorithm for distinguishing gamma-ray interactions from those of fast neutrons in the scintillators is based on the standard charge comparison method, illustrated in Figure 2. Energy information for each trace is extracted using a moving window de-convolution algorithm and the timing of the detector signals is extracted using a digital constant fraction discrimination (CFD) algorithm. The triggerless data acquisition system provides information on individual gamma-ray and neutron energies, timing, and the detector that registered the interaction. Standard RPM observables such as single-gamma and neutron detection rates as well as coincidence rates for gamma–gamma, neutron–neutron, and gamma–neutron events can be derived in real time from the data stream. Typical coincidence time windows are 0–100 ns for gamma–gamma and neutron–neutron events, and 10–100 ns for gamma–neutron events, and can easily be adjusted in the software.

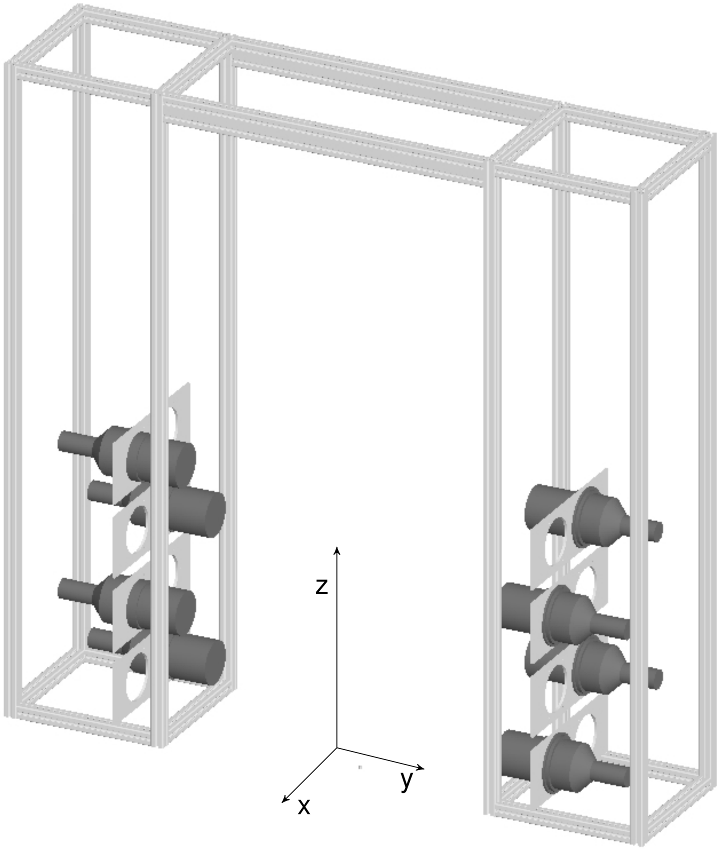

Figure 1. Schematic illustration of the RPM prototype system. In the current configuration, the detector assemblies cover approximately a 100 cm vertical range while the horizontal distance between their front faces is 100 cm as specified in the ANSI N42.35-2016 RPM industry standard.

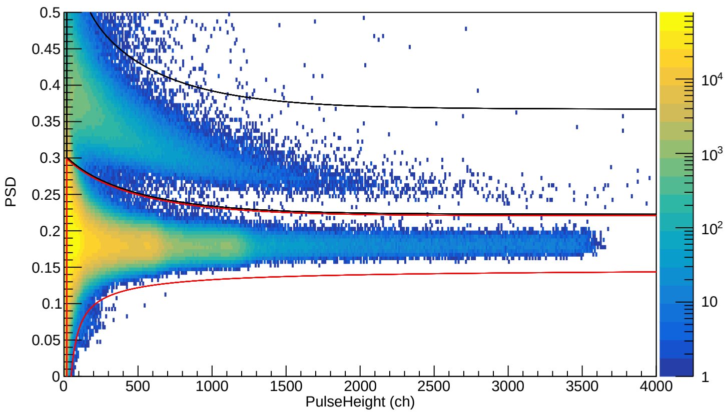

Figure 2. Pulse-shape discrimination plot for one of the eight detector cells in the RPM. The PSD parameter (vertical axis) is the ratio of signal tail charge integral and total charge integral, while the full integrals of the PMT signals are plotted on the horizontal axis. The signals saturate at around 7 MeVee. The number of counts are indicated by the color scale shown on the right side of the plot. Gamma rays and neutrons were selected by choosing events within the regions indicated by the red and black lines, respectively.

2.2. NGET Method

While the main focus of previous studies of systems for SNM detection has been on neutrons, which are a characteristic signature of such materials, there are several advantages connected with the additional detection of gamma rays associated with spontaneous or induced fission. Special and beneficial features of prompt fission gamma rays are their higher multiplicity and short flight time from source to detector. In the fission process, most of the gamma rays are emitted in prompt cascades depopulating short-lived (typically picoseconds–nanoseconds) excited states in the fission products. Therefore, gamma-fast neutron correlations deserve further investigation as an additional SNM detection method, complementing the standard single-gamma and neutron counting, with a potential to significantly reduce RPM false alarm rates (FAR) [11].

Gamma-fast neutron coincidences provide not only an additional, more selective, detection mode but also excellent 3D localization capabilities for SNM using the novel neutron–gamma emission tomography (NGET) [2] technique. Location of SNM using NGET can be obtained by analyzing fast neutron–gamma coincidences event-by-event or cumulative distributions of, primarily, particle arrival time differences using machine learning or statistical methods. Here, results using a Bayesian method applied event-by-event are presented. For each event, the algorithm calculates the probability distribution for the possible points of origin in space from the measured energy deposited by the neutron and the gamma–neutron time difference. Differently from neutron scatter cameras, which can also provide images of SNM, only the detection of one neutron interaction is required while the probability for detection of coincident gamma rays is enhanced due to the much higher prompt fission gamma-ray multiplicity [12]. Since fast neutrons mainly interact via elastic scattering on protons in the organic scintillator, the measured recoil energy samples the incoming neutron kinetic energy and also sets a lower limit of the kinetic energy carried by the incident neutron. Since neutrons emitted from spontaneous fission of SNM have well known energy distributions, often approximated by a Watt spectrum [13], the measured energy deposited by a neutron can be transformed into a probability distribution for the kinetic energy of the incident neutron. Together with the measured time-of-flight (TOF) between the photon and the neutron from the same fission event, the derived neutron energy probability distribution can be transformed into a probability density function for the location of the emission point. For the image reconstruction, a deconvolution algorithm based on Bayes's theorem [14] was applied to the event-by-event data. The performance of the NGET method applied to the KTH Phase I RPM prototype was tested for a ^{252}Cf source in different shielding conditions.

3. RPM Detection Performance Results

3.1. Background Evaluation

According to the ANSI N42.35-2016 reference and standard test conditions, the gamma radiation background should be between 5–10 μR/h and less or equal to 200 background neutrons/s/m^2. Typical RPM systems with ^{3}He counters or similar thermal neutron detectors are sensitive to the full cosmic-ray neutron spectrum, including the down-scattered neutrons. Organic-scintillator based detection systems are, on the other hand, mainly sensitive to fast neutrons and, as a result, the neutron background rates are significantly reduced. The main contribution to the neutron background count rate for organic-scintillator detectors operated with neutron/gamma PSD is caused by particle misidentification where the detector signals are affected by electronic noise or pile-up. This effect is proportional to the average singles gamma rate in the scintillators with a factor typically around one to a few per thousand [15] depending on the PSD cuts applied. The background count rates measured by the KTH RPM prototype system during tests in the Detector laboratory of the KTH Nuclear Physics Division are given in Table 1. The average radiation background dose rate in this environment is around 0.2 μSv/h. The energy thresholds for gamma rays and neutrons were set to 20 keV and around 500 keV, respectively. It is noteworthy that the system was not shielded against background radiation in the presently reported configuration. Standard commercial RPM systems usually have several mm of lead shielding installed on the outer sides, reducing background count rates.

Table 1. Measured background count rates without detector shielding. The energy thresholds for gamma rays and neutrons were 20 keV and around 500 keV, respectively.

	Counts/s
Single γ-rays	5189.0 $\pm$ 0.2
Single neutrons	1.000 $\pm$ 0.002
γ–neutron coinc.	0.0030 $\pm$ 0.0002
γ–γ coinc.	63.00 $\pm$ 0.02
Neutron-neutron coinc.	0.0021 $\pm$ 0.0001

3.2. False Alarm Rate Tests

A "false alarm" is defined when an alarm is triggered due to a measurement of counts in any of the measured parameters (neutrons, gamma-rays, gamma–neutron coincidences, neutron–neutron coincidences, etc.) above a preselected or automatically determined alarm level during the relevant measurement period, while no radiation source other than room background is present. The ANSI N42.35-2016 evaluation standard for RPMs does not take into account detection systems which are able to measure fast particle coincidences, as in the present case. The false alarm test requirements, for both single gamma-rays and neutrons, are less than one alarm per 1000 occupancies for systems with occupancy sensor or one alarm in two hours' measurement time in systems without occupancy sensor [9]. The KTH RPM prototype system can be operated in both modes, i.e., with or without occupancy sensor. The adopted alarm trigger thresholds were set to $\gtrsim 4\sigma$ above mean background count rates and are given in Table 2. These thresholds were decided to be optimal for an interrogation time of one second in the background conditions measured with the KTH RPM prototype system. The detection probability for one gamma-fast neutron coincidence event in a one-second interrogation time due to room background radiation was determined to be 0.003. The system was let to measure background radiation continuously for a total measurement time of 61.4 h, corresponding to a total of 221,000 individual one-second measurements. In only one case during this period were two gamma–neutron coincidence events observed within one second of each other. Consequently, the false alarm rate for fast gamma–neutron coincidence events was determined to be of the order of $4 \times 10^{-6} \mathrm{s}^{-1}$.

Table 2. Adopted alarm trigger thresholds, $\gtrsim 4\sigma$ above mean background count rates.

Detection Mode	**Threshold (Counts/s)**	**Threshold ($\sigma_{\mathbf{B}}$)**
Single γ-rays	5477	4
Single neutrons	5	4
γ-neutron coinc.	1	18
γ-γ coinc.	95	4
Neutron-neutron coinc.	1	21

3.3. Radiation Source Tests

The RPM prototype system was tested for its response to the passage of standard radioactive sources ^{252}Cf, ^{133}Ba, and ^{137}Cs. The sigma multiplier factor N [16] and the false-negative probability, p_N, (i.e., the probability that the passage of the source was not detected) were determined for a one-second interrogation time period. This means that the source moves through the RPM at a speed of 1.2 m/s, covering the distance from -0.6 m to

+0.6 m with respect to the plane through the center of the RPM assembly, as prescribed by the ANSI N42.35-2016 standard [9]. The ANSI N42.35-2016 standard document describes a series of measurements using eight different standard radiation sources, each with its specified activity. We here present the results obtained with two different gamma-ray sources (^{133}Ba and ^{137}Cs) and one neutron source (^{252}Cf). These results are deemed to be representative of the overall performance, especially since the detection threshold of the KTH Imaging RPM prototype system for gamma rays (20 keV) is significantly below the threshold of 40 keV required by the ANSI N42.35-2016 standard.

The passing of each source through the RPM was simulated by means of a series of static measurements covering a range of distances along a line parallel with the x-axis through the center of the RPM, see Figure 1 and Tables 3 and 4. The sigma multiplier factor is defined by the condition that the sum of the mean number of background counts $<C_B>$ and the product of its standard deviation σ_B, and the sigma multiplier factor N, equals the mean counts measured with the source present during a given interrogation time:

$$< C_{\rm B} > +N \times \sigma_{\rm B} \equiv < C_{\rm S+B} > \quad (1)$$

The individual detectors were gain matched using standard calibration sources, using the internal conversion K X-ray photopeak and Compton edge for ^{137}Cs (32 keV and 478 keV, respectively), and the 59.5 keV photopeak of ^{241}Am.

3.3.1. ^{252}Cf

Table 3 summarizes the results of the measured response to the passage of a 1.25 μCi ^{252}Cf source. This relatively weak source had a neutron emission rate of approximately 5400 n/s, which corresponds to 27% of the activity of the ^{252}Cf source prescribed for RPM tests of neutron sensitive RPMs by the ANSI N42.35-2016 standard [9]. The ^{252}Cf material was embedded in a ceramic cylinder with dimensions 4.6 mm (diameter) by 6 mm and encapsulated in a double-welded stainless-steel cylinder with outer dimensions 7.8 mm (diam.) by 10.0 mm. The highest sigma multiplier factor, and hence the lowest FAR was obtained for gamma–neutron coincidence detection whereas the highest statistics and lowest false-negative probability is achieved for single-neutron counting, by far exceeding the requirement of a maximum average false negative probability of $p_N = 1.7\%$ specified by the ANSI N42.35-2016 industry standard. Consequently, the best overall performance of the RPM in terms of combined sensitivity and FAR was obtained from joint single-neutron and gamma–neutron coincidence counting. The last row in the table gives the ANSI N42.35-2016 specified neutron source emission rate and scaled sigma multiplier factors and false negative probabilities that would result from measurements on a source with such an emission rate.

Table 3. Alarm test results for the lab ^{252}Cf neutron source and ANSI N42.35-2016 specified neutron source activity.

^{252}Cf Source Type	Neutrons/s	Single Neutrons N/p_N	γ-Neutron Coinc. N/p_N	Neutron-Neutron Coinc. N/p_N
lab source	5400	$30/9 \times 10^{-9}$	$38/0.13$	$4/0.84$
ANSI N42.35-2016	20,000	$112/3 \times 10^{-41}$	$140/3 \times 10^{-4}$	$14/0.53$

3.3.2. ^{133}Ba and ^{137}Cs

Table 4 shows results of the measured response to the passage of ^{133}Ba and ^{137}Cs gamma-ray sources through the RPM, with activity of 44 kBq and 184 kBq, respectively. These activities correspond to 8.5% and 31% of the ANSI standard activities for these source categories. The radioactive source ^{133}Ba is often used as a "gamma-ray emitting surrogate" for weapons grade plutonium (WGPu). The activity of the ^{133}Ba source used in these measurements only produced an increase of approximately 10% in the single-gamma ray count rate over the normal gamma background rate. With an activity of 120 kBq , it corresponds to approximately 1 g of WGPu. The results showed a high sensitivity for the detection of these weak sources, with a performance largely surpassing the ANSI N42.35-2016 industry standard with its maximum limit on the average false negative probability of $p_N = 1.7\%$. Table 4 also shows the ANSI N42.35-2016 specified gamma source activities and sigma multiplier factors and false-negative probabilities scaled for these activities.

Table 4. Alarm test results for the gamma sources ^{133}Ba and ^{137}Cs as well as corresponding values calculated for ANSI N42.35-2016 specified gamma source activities.

Source Type	Activity (kBq)	Sigma Multiplier Factor N	Probability of False Negative p_N
^{133}Ba lab source	44	8	3×10^{-4}
^{133}Ba ANSI N42.35-2016	518	865	0
^{137}Cs lab source	184	28	0
^{137}Cs ANSI N42.35-2016	592	249	0

4. 3D localization of SNM

As discussed above, the capability to measure fast time correlations between gamma rays and neutrons affords the KTH RPM prototype with an increased sensitivity for detection of small quantities of SNM while maintaining the FAR at a minimum. However, an even more radical consequence of this detection mode is that it enables a simultaneous rapid imaging of SNM in the field of view [2].

The capabilities to locate a ^{252}Cf source using the NGET technique have been studied for a bare source and in different shielding conditions. The ^{252}Cf source, see Section 3.3.1, was oriented with its long axis along z as defined in Figure 1. Shielding was applied by placing the source at the center of plastic and lead cylinders in order to investigate the influence of the shielding on the spatial resolution. The plastic cylinder was manufactured from ultra-high molecular weight polyethylene (PE1000) with 40 mm radial thickness and 83 mm height while the lead cylinder had a 16 mm radial thickness and 105 mm height. Figure 3 shows the results of event-by-event NGET image reconstruction for the bare and shielded 1.25 µCi ^{252}Cf source described in Section 3.3.1. The panels show probability density distributions based on Bayesian inference projected on the $y - z$ plane. The data was acquired for three different positions of the source; (x, y, z) = (0, −30, 22) cm, (0, 0, 52) cm, and (0, 30, 82) cm, each during a 10 s measurement time. Figure 4 illustrates the resulting 3D-representation of the source inside the plastic cylinder with 2D-projections on the $x - y$, $x - z$ and $y - z$ planes.

In order to evaluate the spatial resolution of the system the NGET algorithm was applied in 1800 different 10 s measurements. The 1.25 µCi ^{252}Cf source was placed in the central position (x, y, z) = (0, 0, 52) cm, without shielding and with PE1000 and lead shielding, respectively. Table 5 specifies spatial resolution (σ_{xyz}) obtained from Figure 5. Figure 5 shows projections on the x, y, and z axes of the three-dimensional spatial distributions of the most probable source position obtained in each 10 s measurement.

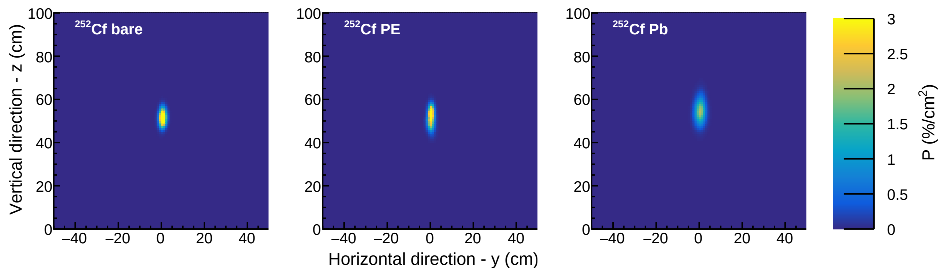

Figure 3. Source localization results based on Bayesian inference applied to event-by-event data. Each panel corresponds to a 10 s measurement of the 1.25 µCi ^{252}Cf source. The source was placed at $(x, y, z) = (0, 0, 52)$ cm. The image panels show projected probability density distributions in the $y - z$ plane for the bare source (**left**), inside the PE1000 shielding (**middle**), and inside the lead shielding (**right**). The estimated probability of finding the source per cm^2 pixel is indicated by the color scale on the right. See text for details.

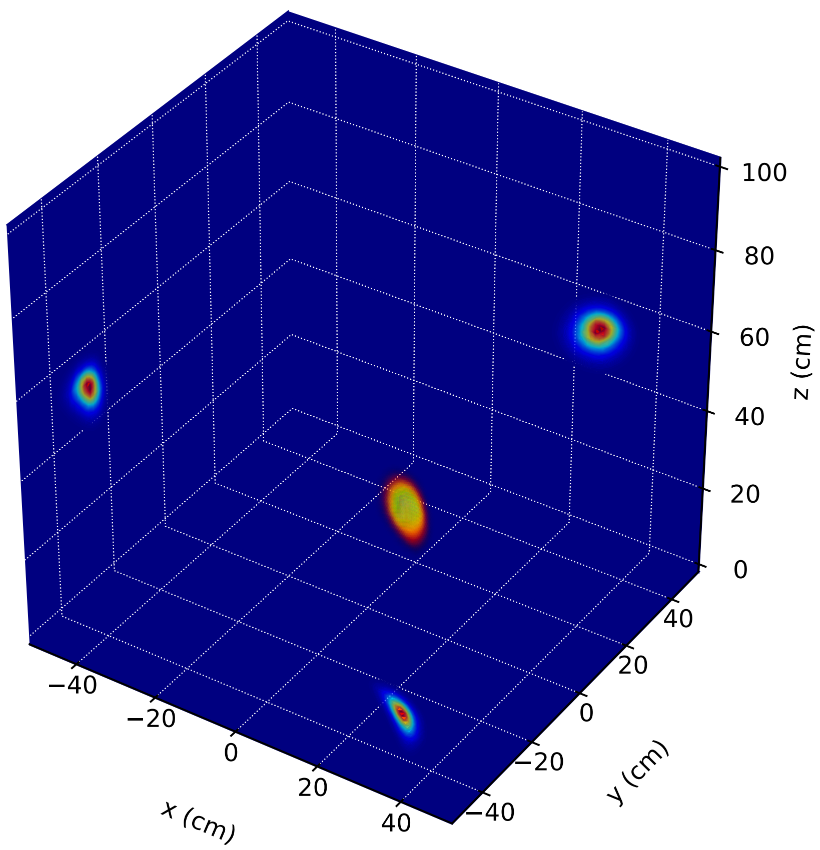

Figure 4. 3D representation of the localization of the 1.25 µCi ^{252}Cf source shielded with the lead cylinder, with projections in the xy, xz, and yz planes. The source was placed at a position $(x, y, z) = (30, -30, 52)$ cm. The measurement time used for producing the image was 10 s.

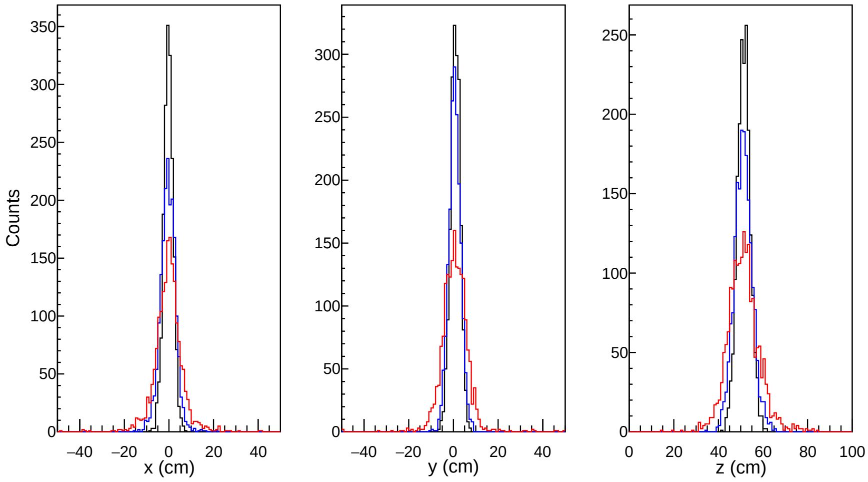

Figure 5. Spatial resolution obtained from event-by-event NGET image reconstruction of the ^{252}Cf source. The results were obtained for 1800 different 10 s measurements. The three panels show projections of the three-dimensional spatial distributions on the x, y, and z axes of the most probable source position determined in each measurement. Results are given for the bare source (black line) and inside PE1000 and lead shielding (blue and red line, respectively). The ^{252}Cf source was kept fixed in the position $(x, y, z) = (0, 0, 52)$ cm during the measurements.

Table 5. Spatial resolution (σ_{xyz}) obtained from 1800 10-second measurements of the 1.25 µCi ^{252}Cf source.

	σ_x	σ_y	σ_z
bare ^{252}Cf	2.09 ± 0.04	2.16 ± 0.04	2.89 ± 0.05
^{252}Cf + PE1000	3.20 ± 0.07	2.65 ± 0.05	3.97 ± 0.08
^{252}Cf + lead	4.8 ± 0.2	4.76 ± 0.09	6.2 ± 0.2

5. Discussion

Rapid and efficient detection of nuclear and other radioactive materials using radiation portal monitors constitutes one of the critical links in the global efforts against nuclear terrorism and the proliferation of nuclear weapons. Additionally, the possibility of rapid, precise, and automatic location of SNM detected at security checkpoints would tremendously speed up the response time and reduce or remove the need for on-site personnel trained in radiation detection. It would also enable potentially critical time savings for nuclear emergency responders and facilitate the work of safeguards inspectors. It has been demonstrated that by adding the capabilities to measure detailed correlations in time and space between gamma rays and fast neutrons from nuclear fission in an RPM system based on an array of organic scintillators, an increased sensitivity and selectivity for the notoriously elusive SNM, such as plutonium, can be achieved while maintaining FAR at a very low level. Using the NGET imaging modality, such a detection system is then also capable of rapidly and precisely locating SNM within the field of view. Based on these principles, an imaging RPM prototype system suitable for pedestrian and package (or conveyor) screening has been designed and tested at KTH Royal Institute of Technology. The novel imaging method has superior performance in terms of spatial resolution and detection efficiency [2] compared with neutron scatter imaging (see, e.g., Ref. [17]). The spatial resolution from around 2 up to a few cm obtained in this work is remarkable considering the several times larger dimensions of the detector cells used in the current version of the Phase I KTH RPM prototype system. The results also indicate a robustness of the NGET imaging technique against the presence of moderate amounts of shielding materials of different types. Future developments of the imaging RPM concept will include comprehensive studies of the localization capabilities for sources placed inside a variety of shielding materials and matrices, as well as further optimization of the image reconstruction of multiple and spatially distributed sources.

6. Patents

B.C. is the inventor on patent applications related to this work filed by KTH Holding AB, KTH Royal Institute of Technology (Nos. US 17/255143, EP 3811121, CN 201980043247.2).

Author Contributions: Conceptualization, B.C.; methodology, B.C. and J.V.; software, J.V.; validation, B.C. and J.V.; formal analysis, B.C. and J.V.; investigation, B.C. and J.V.; resources, B.C.; data curation, J.V.; writing—original draft preparation, B.C. and J.V.; writing—review and editing, B.C. and J.V.; visualization, J.V.; supervision, B.C.; project administration, B.C.; funding acquisition, B.C. All authors have read and agreed to the published version of the manuscript.

Funding: This work has received funding from the Swedish Radiation Safety Authority under contract nos. SSM2016-3954, SSM2018-4393, and SSM2018-4972 and the Carl Trygger Foundation for Scientific Research under contract no. CTS14:89.

Institutional Review Board Statement: Not applicable.

Informed Consent Statement: Not applicable.

Data Availability Statement: All data needed to evaluate the conclusions in the paper are present in the paper and/or the Supplementary Materials. Data used in generating the main figures are available at Zenodo (DOI: 10.5281/zenodo.7007278).

Acknowledgments: Software development support from A. Göök is acknowledged.

Conflicts of Interest: The authors declare no conflict of interest. The funders had no role in the design of the study; in the collection, analyses, or interpretation of data; in the writing of the manuscript; or in the decision to publish the results.

References

1. Iaea Incident and Trafficking Database (ITDB). *Incidents of Nuclear and Other Radioactive Material Out of Regulatory Control 2020 Fact Sheet*; IAEA Incident and Trafficking Database (ITDB): Vienna, Austria, 2020.
2. Petrović, J.; Göök, A.; Cederwall, B. Rapid imaging of special nuclear materials for nuclear nonproliferation and terrorism prevention. *Sci. Adv.* **2021**, *7*, eabg3032. [CrossRef] [PubMed]
3. Stone, R. New type of imager could help spot smuggled nuclear materials. *Science*, 19 May 2021. [CrossRef]
4. Ensslin, N.; Harker, W.; Krick, M.; Langner, D.; Pickrell, M.; Stewart, J. *Application Guide to Neutron Multiplicity Counting*; Los Alamos Report LA-13422- M; Los Alamos National Laboratory: Los Alamos, NM, USA, 1998.
5. Menlove, H.O.; Swansen, J.E. A High-Performance Neutron Time Correlation Counter. *Nucl. Technol.* **1985**, *71*, 497–505. [CrossRef]
6. Pickrell, M.M.; Lavietes, A.D.; Gavron, V.; Henzlova, D.; Joyce, M.J.; Kouzes, R.T.; Menlov, H.O. The IAEA Workshop on Requirements and Potential Technologies for Replacement of ^{3}He Detectors in IAEA Safeguards Applications. *J. Inst. Nucl. Mater. Manag.* **2013**, *41*, 14–29.
7. Lewis, J.M.; Kelley, R.P.; Murer, D.; Jordan, K.A. Fission signal detection using helium-4 gas fast neutron scintillation detectors. *Appl. Phys. Lett.* **2014**, *105*, 014102. [CrossRef]
8. Pozzi, S.; Clarke, S.; Paff, M.; Di Fulvio, A.; Kouzes, R. Comparative neutron detection efficiency in He-3 proportional counters and liquid scintillators. *Nucl. Instrum. Methods Phys. Res. Sect. Accel. Spectrometers Detect. Assoc. Equip.* **2019**, *929*, 107–112. [CrossRef]
9. *American National Standard for Evaluation and Performance of Radiation Detection Portal Monitors for Use in Homeland Security*; IEEE: Piscataway, NJ, USA, 2016. [CrossRef]
10. Eljen Technology, Neutron/Gamma PSD liquid Scintillator EJ-301, EJ-309. Available online: https://eljentechnology.com/products/liquid-scintillators/ej-301-ej-309 (accessed on 15 August 2022).
11. Trombetta, D.; Sundaram, C.; Axell, K.; Cederwall, B. Sensitive Detection of Special Nuclear Materials Based on gamma-fast neutron Coincidence Counting for RPM Applications. In Proceedings of the International Conference on Nuclear Security, Vienna, Austria, 10–14 February 2020; Volume 8710.
12. Trombetta, D.M.; Klintefjord, M.; Axell, K.; Cederwall, B. Fast neutron- and γ-ray coincidence detection for nuclear security and safeguards applications. *Nucl. Instrum. Methods Phys. Res. Sect. Accel. Spectrometers Detect. Assoc. Equip.* **2019**, *927*, 119–124. [CrossRef]

13. Watt, B.E. Energy Spectrum of Neutrons from Thermal Fission of U^{235}. *Phys. Rev.* **1952**, *87*, 1037–1041. [CrossRef]
14. D'Agostini, G. A Multidimensional unfolding method based on Bayes' theorem. *Nucl. Instrum. Meth. A* **1995**, *362*, 487–498. [CrossRef]
15. Cederkäll, J.; Cederwall, B.; Johnson, A.; Palacz, M. Relative enhancement of weak two-neutron exit channels in heavy-ion induced fusion-evaporation reactions. *Nucl. Instrum. Methods Phys. Res. Sect. Accel. Spectrometers Detect. Assoc. Equip.* **1997**, *385*, 166–170. [CrossRef]
16. *Technical and Functional Specifications for Border Monitoring Equipment*; Number 1 in Technical Guidance; International Atomic Energy Agency: Vienna, Austria, 2016.
17. Steinberger, W.M.; Ruch, M.L.; Giha, N.; Fulvio, A.D.; Marleau, P.; Clarke, S.D.; Pozzi, S.A. Imaging Special Nuclear Material using a Handheld Dual Particle Imager. *Sci. Rep.* **2020**, *10*, 1855. [CrossRef] [PubMed]